This article has been accepted for publication in IEEE Sensors Journal. This is the author's version which has not been fully edited and content may change prior to final publication. Citation information: DOI 10.1109/JSEN.2024.3506037

Chandrayaan-3 LIBS Sensor: Pre-flight Characterization, Inflight Operations and Preliminary Observations

R.V.L.N. Sridhar, Adwaita Goswami, K.A. Lohar, S. Malathi and K.V. Sriram

***Abstract*— The Laser Induced Breakdown Spectroscopy (LIBS) sensor on the Chandrayaan-3 rover, Pragyaan, is the maiden LIBS technique-based instrument to operate on the airless planetary body, the Moon. This miniaturized Low-energy Eye-safe LIBS (LE-LIBS) instrument performs in-situ elemental investigations on the lunar surface from a close distance of 0.2 meters. The LE-LIBS instrument is equipped with a compact Yb:Er:Glass 1.54 μm pulsed laser for material surface ablation and a free-space optics-coupled flat-field spectrometer to record the micro-plasma emission. Before the voyage, the flight instrument was characterized to assess its performance as a function of operating conditions, viz., temperature, working distance, sample form, etc., in high vacuum. Performed first-cut univariate analysis resulted in <5% uncertainty in elemental abundance estimation. Over 740 LIBS spectra of the lunar-regolith are recorded at 25 different sites surrounding the 'Shiv Shakti' point in the southern high latitude on the Moon. Preliminary analysis of the LIBS spectra recorded in regions a few meters away from the landing point has indicated the presence of elements, viz., O, Mg, Al, Si, Ca, Fe, Ti, Mn, Cr, etc., hinting at the possible presence of Ca, Al-rich silicate minerals, and low-Ti magnesium iron silicate minerals. In this paper, we report salient engineering details of the instrument, pre-flight characterization, inflight functionality, and preliminary performance aspects.**

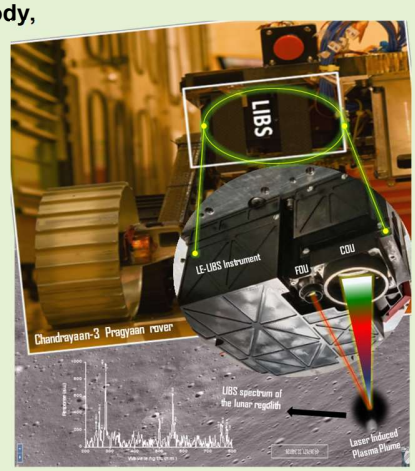

***Index Terms*—In-situ close-range LIBS, elemental analysis, Yb:Er:Glass laser, Chandrayaan-3, Moon, Space science**

I. Introduction

The capability of in-situ analytical methods to probe planetary surfaces in harsh and hands-off conditions is advancing rapidly [1-4]. In-situ robotic or rover platform measurements in conjunction with the global observations of orbital craft platforms can provide a comprehensive understanding of the planetary surface chemistry. Amongst several kinds of in-situ analytical techniques, the Optical Emission Spectroscopy (OES) technique, namely, the laser-induced breakdown spectroscopy (LIBS) [5], is gaining rejuvenated interest in recent times. The LIBS technique offers rapid, simultaneous multi-elemental detection and is sensitive to lighter elements, including hydrogen. In principle, this OES technique employs a high-power density laser beam to ablate the sample surface. Thus, the generated microplasma is analyzed spectroscopically for the elemental composition of the target sample. Owing to its versatility and advantages over the laborious and long-time-consuming proximity or contact conventional methods, the LIBS technique has become a potential field of both fundamental and exploratory research [6-8], including space sciences [9-12].

The applicability of the LIBS technique for planetary surface chemistry necessitates a special attention, as the plume dynamics is influenced by low-pressure conditions in contrast to the terrestrial environment. Several research groups have performed numerical modelling simulations and experiments at ambient pressures ranging from 500 Pa to 10^{-5} Pa to understand the ablation kinetics, plume dynamics, spectral response, and detection limits [9, 13-17]. Despite the low-signal characteristics expected due to the lateral expansion of the plume expansion at low pressures of $\leq 10^{-5}$ Pa, the work reported by J. Lasue *et al.* [13], R. Shu *et al.* [15], B. Sallé *et al.* [16], and F. Colalo *et al.* [11] exhibited the LIBS technique's suitability for planetary surface exploration. These methodological aspects, combined with mission resources and constrains in terms of mass, power, volume, operating temperature, vibrational shocks, robustness, etc., pose major engineering challenges in the development of a space-compatible LIBS instrument. The first-ever instrument built on the laser-induced breakdown spectroscopy technique is the

Corresponding author: R.V.L.N. Sridhar is the Principal Investigator of the LE-LIBS instrument on the Chandrayaan-3 rover, Laboratory for Electro-Optics Systems (LEOS), Indian Space Research Organization (ISRO), Bengaluru, India, 560058, and is the Research Scholar of M.S. Ramaiah University of Applied Sciences, Bengaluru. (email: rvlnsridhar@leos.gov.in, yourssriraj@gmail.com)
Co-authors: Adwaita Goswami, K.A. Lohar and K.V. Sriram are with the Laboratory for Electro-Optics Systems (LEOS), ISRO, Bengaluru, India (e-mail: adwaita@leos.gov.in, lohar_ka@leos.gov.in, drkvs@leos.gov.in).
Prof. S. Malathi is with the Graphic Era (Deemed to be) University, Dehradun, India, 248002, (email: s.malathi.ece@geu.ac.in)

XXXX-XXXX © XXXX IEEE. Personal use is permitted, but republication/redistribution requires IEEE permission.
See http://www.ieee.org/publications_standards/publications/rights/index.html for more information.

Authorized licensed use limited to: KIIT University. Downloaded on December 05,2024 at 14:49:34 UTC from IEEE Xplore. Restrictions apply.
© 2024 IEEE. Personal use is permitted, but republication/redistribution requires IEEE permission. See https://www.ieee.org/publications/rights/index.html for more information.

This article has been accepted for publication in IEEE Sensors Journal. This is the author's version which has not been fully edited and content may change prior to final publication. Citation information: DOI 10.1109/JSEN.2024.3506037

'ChemCam' [18] aboard the 'Curiosity rover' in NASA's Mars Science Laboratory mission. From its first LIBS spectral acquisition in the Gale Crater on Mars in 2012 to till date, the ChemCam has successfully recorded more than 0.9 million single-shot LIBS spectra and has been providing invaluable scientific information. The other two currently active rovers that are equipped with LIBS instruments for the Martian surface exploration are, the 'SuperCam' [19] on the Perseverance Mars 2020 rover at Jezero Crater and the 'MarSCoDe' [20] on the Zhurong rover that successfully landed on the southern Utopia Planitia of Mars in the year 2021 by the CNSA. While these three LIBS systems are currently in action to explore the Martian surface chemistry, the voyage of the first LIBS instrument to the Moon was on the Pragyaan rover in ISRO's Chandrayaan-2 mission in the year 2019 [21]. Among all other planetary chemistry analytical instruments, this instrument has the lowest analytical spot size (100 μm diameter), permitting the observation of individual grains. However, due to the hard landing of the lander craft the instrument could not able to operate. A similar kind of instrument, named LE-LIBS (low-energy eye-safe LIBS) with performance improvements flown in India's subsequent lunar mission, Chandrayaan-3. The VOILA (Volatiles Identification by Laser Analysis) is another LIBS instrument, that is currently in the developing phase for the LUVMI-X Rover, aiming for volatile detection in the lunar polar region [22].

Though LIBS is a versatile technique, it suffers from low reproducibility and repeatability due to unknown chemical matrix effects, whose occurrence can be due to several factors like the physical properties of the target, such as grain size, surface roughness, thermal conductivity and absorptivity, sample ablation kinetics, and coupling efficiency [23, 24]. In addition, as mentioned above, LIBS is sensitive to ambient environment and working conditions, viz., temperature, atmospheric pressure, sample to instrument distance, etc., which will affect the plasma plume dynamics and emission signal strength. Knight *et al.* [9] showed stronger emission line intensities at the pressure level characteristics of the Martian environment in comparison to those measurements performed at terrestrial pressure levels. The work of Jobin K. Antony *et al.* [14] and R. Shu *et al.* [15] demonstrated the LIBS emission signal detection at lower pressure levels in the range of 10^{-4} Pa to 10^{-5} Pa. One of the major challenges of LIBS instrument development having all above-specified investigation prospects is its functionality and performance validation in environmental conditions mimicking those of the targeted planetary body. The subsequent challenge dwells in the reliable calibration and characterization of the instrument to generate correlation and correction factors for pixel-to-wavelength conversion, wavelength-dependent instrument response, temperature-dependent pixel shift, and a spectra database employing standard/certified reference material samples. R.C. Wiens *et al.* [25], L. Carey *et al*. [26], X. Liu *et al.* [27] reported details on diverse adapted strategies and limitations associated with the pre-flight calibration of LIBS instruments flown on the Curiosity Rover, Perseverance Rover, and the Zhurong Rover. In our work, prior to the integration of the instrument with the rover, laser-induced plasma emission spectra were acquired in a high vacuum environment from a set of 40 geochemically certified reference material (CRM) samples that comprise elemental oxides varying in composition. These spectra were subjected to the data-preprocessing approach to produce clean spectra (spectra free from the background, random noise, and baseline continuum). The LE-LIBS instrument on the Pragyaan rover, Chandrayaan-3, operated successfully for 9-earth days since its first LIBS measurement of the lunar regolith on 25 August 2023. This paper provides an overview of salient engineering details of the instrument, calibration and characterization methodology, and the elemental composition analytical strategy. Additionally, this paper reports a short discussion on functionality and the preliminary performance aspects of the LE-LIBS instrument on the Moon.

II. LE-LIBS Instrument on Chandrayaan-3 Rover

Chandrayaan-3 [28], the third Indian mission to the Moon, had successfully soft-landed a craft named Vikram on a much-unexplored region (latitude: 69.367° south, longitude: 32.348° east) located in the southern high latitudes of the moon. The Vikram lander-craft enfolded a six-wheeled Pragyaan rover that had smoothly rolled down to the lunar surface on August 24, 2023. The LE-LIBS instrument shown in Fig. 1. is one of the two scientific payloads on the rover, developed with the scientific motive of executing in situ close-range elemental investigations on the lunar surface. Its prime technological objective is to demonstrate and assess the LIBS capability in an airless environment. Based on the available footprint, mass, and power resources of the rover, this instrument was configured to be of a low mass (≤1.2 kg) and low power (≤ 1.5 W, steady state) consuming compact (total volume of ≤ 2 liters) system. The instrument was housed to the bottom chassis of the rover, looking down towards the lunar surface. The two optical viewports on the bottom-left corner of Fig. 1. are the collection optics unit (COU) and the ablation optics unit (AOU), whose optical axes converge at a distance of 200 mm with respect to the last lens of the AOU. The focused laser beam transmitting from the AOU (the smaller viewport in Fig. 1.) is incident on the lunar surface at an oblique angle of 10°, while the COU axis is perpendicular to the target. A miniaturized solid-state q-switch laser *(L3Harris®)* emitting the 1535 nm wavelength radiation with pulse energy of ~4 mJ at 5 Hz repetition rate is used for the material ablation.

Fig. 1. LE-LIBS instrument aboard the Chandrayaan-3 rover

XXXX-XXXX © XXXX IEEE. Personal use is permitted, but republication/redistribution requires IEEE permission.
See http://www.ieee.org/publications_standards/publications/rights/index.html for more information.

Authorized licensed use limited to: KIIT University. Downloaded on December 05,2024 at 14:49:34 UTC from IEEE Xplore. Restrictions apply.
© 2024 IEEE. Personal use is permitted, but republication/redistribution requires IEEE permission. See https://www.ieee.org/publications/rights/index.html for more information.

This article has been accepted for publication in IEEE Sensors Journal. This is the author's version which has not been fully edited and content may change prior to final publication. Citation information: DOI 10.1109/JSEN.2024.3506037

TABLE I
SPECIFICATIONS OF THE LE-LIBS INSTRUMENT

Parameter	Specification
Laser Pulse Duration	6 ns
M^2 (Beam Quality) Factor	≤ 1.7
Ablation Optics Unit (AOU)	3-lens system
Collection Optics Unit Type	Free-space, lens-coupled
Working Distance (WD)	200 mm ± 8 mm from the AOU
Power Density @ WD	5.5 x 10^{13} W/m^2
Spectral Range	220 nm – 800 nm
Slit Size	50µm (w) x 500µm (h)
Grating F/No.	2.2
Detector Pixel Size	14 µm (w) x 200 µm (h)
Optical Resolution (FWHM)	≤1.1 nm
Instrument Dimensions	180 mm (l) x 150 mm (w) x 80 mm (h)
Operating Temperature	- 15 ^{0}C to + 55 ^{0}C
Data Size	25 kbps/single-laser shot spectrum
Acquisition Delay and Integration time	Programmable (delay time: 0.25 µs – 5 µs; integration time: 8 µs – 9 ms)
Spectral Acquisition Sequence	Non-laser background spectrum, laser-induced plasma emission spectrum

Er^{3+}/Yb^{3+} phosphate glass laser was chosen for this instrument, because of its improved gain characteristics, eye-safe wavelength, peak power, and most importantly, its smaller size, low weight, wide-operating temperature range without any TEC, and excellent beam quality [29, 30]. In recent times, these compact eye-safe wavelength lasers are receiving a great deal of interest for their use in LiDAR, optical communication, and spectroscopy [31, 32]. Moreover, in LIBS methodology, longer wavelength (> 1 µm) lasers can result in a more efficient plasma excitation and have advantages in plasma formation and coupling. These lasers having excellent beam quality and short pulse duration are more favorable since they heat up the microplasma at a slower rate and generate a larger and less dense plume, leading to strong emission lines [33, 34]. A.S. Laxmiprasad *et al.* [35] reported the ablation dynamics and plasma emissivity prospects from a modest, low-energy, and 1535 nm laser excitation-based LIBS instrument. The LE-LIBS instrument comprised an in-house developed flat-field spectrometer equipped with a 50-µm width rectangular slit *(Liberty International)*, an aberration-corrected concave holographic reflective grating *(Spectrum Scientific, Inc.)*, and an UV-enhanced 2048-element linear CCD (*Toshiba*) as the detector. Table I presents the salient specifications of the LE-LIBS instrument on the Chandrayaan-3 Pragyaan rover. Prior to the integration with the rover, the instrument was subjected to rigorous environmental and dynamic tests, namely, thermo-vacuum (-15 °C to + 55 °C) cycling, shock (700g in the1000 Hz-5000 Hz range), vibration (18.1 g), and EMI/EMC tests to assess and qualify its functionality for the intended use. In addition to these evaluation tests, it underwent calibration and characterization tests in ambient air and high-vacuum environments at pressure levels of ≤ 1.2 x 10^{-4} Pa employing calibration lamps and geochemical standard certified reference material (CRM) samples to generate correlation factors, instrument response functions, and reference spectral databases. Subsequent sections of the paper report these aspects. On 25 August 2023, the LE-LIBS instrument recorded the first laser-induced plasma emission spectrum of the lunar regolith in a site a couple of meters away from the landing location in the southern high latitude region. Nearly 750 LIBS emission spectra were recorded at different sites nearby the Chandrayaan-3's lander craft landing point, 'Shiv Shakti'. This paper reports an overview of the instrument's functionality and preliminary performance aspects of the instrument aboard the Pragyaan rover on the Moon.

III. Pre-flight Characterization Experiments

The instrument had undergone sequential functionality and performance investigations, namely, spectrometric calibration, intensity calibration, thermal characterization, working distance dependency, sample's form (pellet, loose grains), generation of reference database in a high-vacuum environment, etc. Pre-processing methodology, curve fitting, and peak finding approaches adopted in our data analytical approach, reported elsewhere [36, 37].

A. Wavelength (Spectrometric) Calibration

The spectrometric calibration of the instrument performed using a calibrated mercury-argon (HgAr) lamp (*Avalight-CAL, Avantes*). The calibration test-setup (see Fig. 2.) comprised an 8-inch off-axis collimator *(Santa Barbara Infrared Inc.)*, which sends the collimated HgAr lamp output to the LIBS instrument. The instrument was co-aligned to the collimator's optical axis. The calibrated source emission was captured after a 20-minute warmup time of the lamp. The computed peak centroids (to a fraction of a pixel) of the lamp spectrum recorded by the instrument, and the reported peak wavelengths of the calibration source spectrum are subjected to correlation analysis by means of a multi-linear regression approach. The formula relating the pixel number (p) with the respective wavelength (λ_p) as a third-order polynomial is given below.

$$\lambda_p = a + c_1 * p + c_2 * p^2 + c_3 * p^3 \qquad (1),$$

where λ is the wavelength of pixel 'p, '*a'* is the intercept of the regression-fit that corresponds to the wavelength of the 0^{th} pixel, c_1 is the first coefficient (nm/pixel), c_2 is the second coefficient (nm/$pixel^2$), and c_3 is the third coefficient (nm/$pixel^3$). The LE-LIBS sensor can resolve peaks at approximately 3.6 pixels full width half maximum (FWHM). The applied regression resulted in a near unity (0.999) coefficient of determination (R^2), and a minimal variation (λ_r-λ_p) between the predicted (λ_p) and reference peak wavelength (λ_r). Fig. 3. presents the plot of 'λ_p' and 'λ_r-λ_p' with respect to λ_r. The variations are marked at the ends of the vertical rectangular bars, while the black dots represent the regression-predicted peak wavelengths. The resulting variations are +0.07/-0.03 nm in the MUV window, +0.05/-0.01 nm in the VIS window, and +0.003/-0.007 nm in the NIR window.

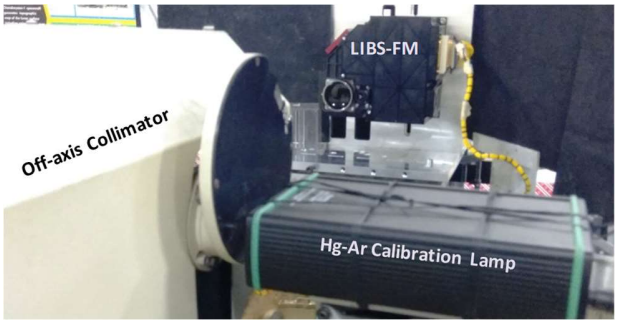

Fig. 2. Spectrometric calibration test setup

XXXX-XXXX © XXXX IEEE. Personal use is permitted, but republication/redistribution requires IEEE permission.
See http://www.ieee.org/publications_standards/publications/rights/index.html for more information.

Authorized licensed use limited to: KIIT University. Downloaded on December 05,2024 at 14:49:34 UTC from IEEE Xplore. Restrictions apply.
© 2024 IEEE. Personal use is permitted, but republication/redistribution requires IEEE permission. See https://www.ieee.org/publications/rights/index.html for more information.

This article has been accepted for publication in IEEE Sensors Journal. This is the author's version which has not been fully edited and content may change prior to final publication. Citation information: DOI 10.1109/JSEN.2024.3506037

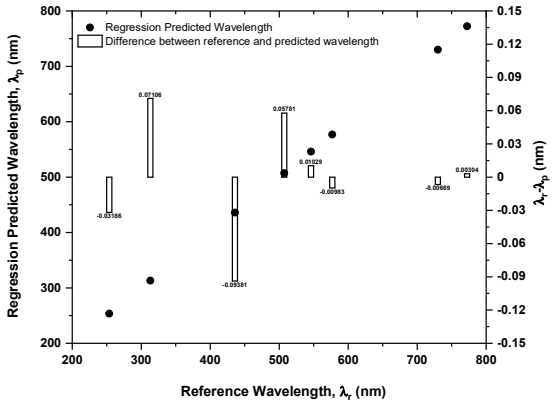
Regression Predicted Wavelength
Difference between reference and predicted wavelength
Regression Predicted Wavelength, λp (nm)
λr-λp (nm)
Reference Wavelength, λr (nm)

Fig. 3. Predicted versus reference line wavelengths

B. Instrument Response Calibration

The wavelength-dependent response curve (transfer function) for the LE-LIBS instrument is generated based on the procedure [38, 39] that compares the instrument recorded signal response (A/D counts/nm) from a calibrated broadband continuum light source radiation output with that of the calibrated source radiance spectrum (μW/cm^2/nm). In our work, we used a calibrated and balanced deuterium-halogen (DH) light source *(Avalight-DH-BAL-CAL, Avantes)* that can emit the radiation in the wavelength range of 200 nm-1100 nm. The source is equipped with a built-in diffuser and a cosine corrector (CC-VIS/NIR). A 'white' (source ON) and 'dark/background' (source OFF) spectral response (A/D counts) are acquired with the instrument after a 40-minute lamp stabilization time. Fig. 4. shows the overlapped normalized response plot of the calibrated DH lamp spectrum (blue line, provided by the manufacturer) and the background response subtracted DH lamp spectrum (red line) as recorded by the instrument. Fig. 4 depicts the presence of low-intense, sharp Balmer lines of deuterium, viz., D_α and D_β, at wavelengths of 486 nm and 655 nm in the reference source spectrum as well as in the instrument's recorded spectrum. The wavelength-dependent response curve (transfer function) is generated using formula (2).

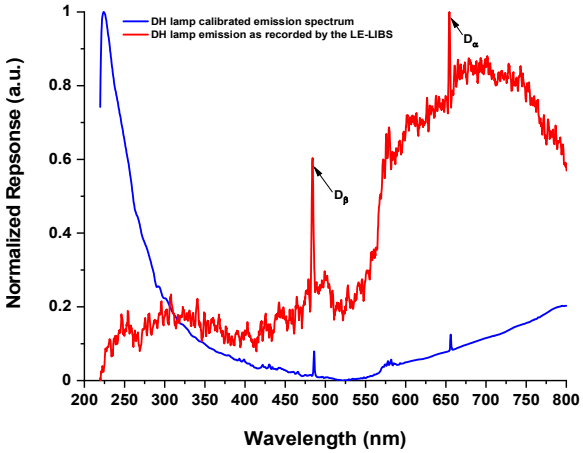

Fig. 4. Normalized response plot *(blue line)* of the reference source spectrum and the LE-LIBS recorded source spectrum *(red line)*

$$TF_n = \frac{Caldata_n}{(refcal_n - darkca\ _n)} \qquad (2),$$

where 'TF_n' is the transfer function, '$Caldata_n$' is the calibrated radiance of the light source at wavelength 'n' in μW/cm^2/nm, '$refcal_n$' and '$darkcal_n$' are the A/D (analog to digital) counts at wavelength 'n' that are recorded by the instrument with the DH-source 'ON' and DH-source OFF. The empirical expression used to compute the radiance (μW/cm^2) from the measured plasma emission response (A/D counts) of the sample is given in formula (3).

$$I_n = TF_n * \left(Sample_{signal\_n} - Sample_{dark\_n}\right) * f \qquad (3),$$

where 'I_n' is the radiance at nth wavelength, '$Sample_{signal\_n}$' is the A/D counts at wavelength 'n' recorded for the laser-induced plasma emission from the target sample, '$Sample_{dark\_n}$' is the A/D counts at wavelength 'n' recorded for the non-laser background, and 'f' is the ratio of the integration times used for $refcal_n$ and $Sample_{signal\_n}$, respectively.

C. Investigations based on the Operating Temperature, Working Distance and the Sample Form

The functionality and performance of the instrument were investigated in a high-vacuum environment as a function of parameters, namely, the instrument's base temperature, working distance, and the target sample's nature. Fig. 5. presents an in-house realized test bench in a TVC (thermo-vacuum) chamber to evaluate and characterize the instrument's functionality as a function of the operating temperature. As shown in the figure, the test setup comprises the LE-LIBS instrument housed to an aluminum-alloy metal sheet (the baseplate) in downward-looking geometry (equivalent to the adapted mounting scheme in the Pragyaan's rover). NCT bead-type thermistors are bonded to the baseplate to monitor and record the operating temperature. A pressed powder disc made from geochemical CRM soil powder *(SX67-05, Brammer Standard Company, Inc.)* at a working distance (height) of 205 mm from the COU is kept inside a sample holder plate. The sample holder plate is mounted to a motorized ultra-high vacuum XY translation stage platform. This platform interfaced to an external controller unit aids in changing the analytical spot position on the sample during investigations. The whole test bench was placed inside a 1.2-meter-diameter TVC chamber at pressure levels of ~ 1.2 x 10^{-4} Pa during the thermal cycling investigations within the operational temperature range (-15 °C to +55 °C) of the instrument. Instrument was exposed to short duration (2 hours) and long duration (24 hours) thermo-vacuum cycles for the designed low and high operational temperatures as mentioned in Table I. The plasma emission spectra (average of 15 spectrums acquired from 3 different sites on the pressed powder sample during each cycle) in high vacuum at temperatures of -15 °C, +25 °C, and +55 °C were used in analyzing the wavelength drift, if any. Figure 6(a) and Figure 6(b) shows overlapped laser-induced plasma emission spectral response plots of the sample in the mid-UV region (270 nm to 285 nm) and near-IR region (790 nm to 798 nm) at three temperatures: -15 °C (black line), +25 °C (red line), and +55 °C (blue line), respectively. We have observed a 12-pixel shift over 71 °C in the mid-UV spectral window, and a 10-pixel shift over 71 °C in the near-IR region of the spectrum. The overall measured (including the VIS spectral region) shift in peaks per °C is ≤ 0.15 pixel.

XXXX-XXXX © XXXX IEEE. Personal use is permitted, but republication/redistribution requires IEEE permission.
See http://www.ieee.org/publications_standards/publications/rights/index.html for more information.

Authorized licensed use limited to: KIIT University. Downloaded on December 05,2024 at 14:49:34 UTC from IEEE Xplore. Restrictions apply.
© 2024 IEEE. Personal use is permitted, but republication/redistribution requires IEEE permission. See https://www.ieee.org/publications/rights/index.html for more information.

This article has been accepted for publication in IEEE Sensors Journal. This is the author's version which has not been fully edited and content may change prior to final publication. Citation information: DOI 10.1109/JSEN.2024.3506037

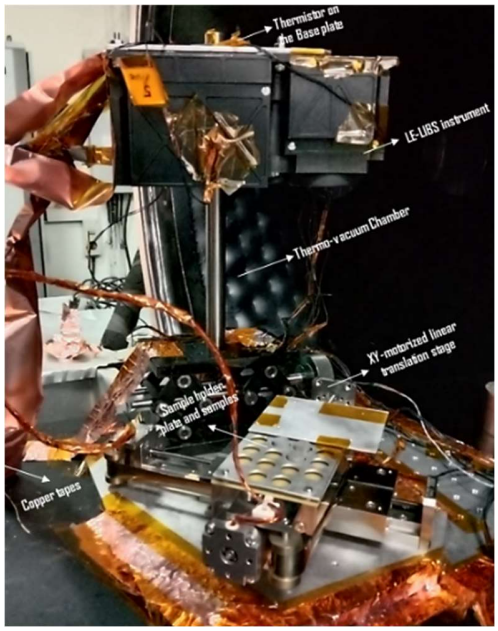

Fig. 5. Characterization test setup in the TVC chamber

The wavelength drift per °C in six spectral windows over the spectral range is fitted to a second-order degree polynomial. Formula (4) is an empirical expression formulated for the correction of the temperature-dependent wavelength-drift of the instrument.

$$\lambda_{corrected} = \lambda_{measured} + \left[\Delta T\left(0.0512 + 3.95e-5 * \lambda_{measured} - 5.63e-8 * \lambda_{measured}^{2}\right)\right] \quad (4),$$

where, $\Delta T = T_{base} - 25$ (T_{base} is the recorded baseplate temperature in °C during the instrument operation) and '$\lambda_{measured}$' is the wavelength window of the recorded spectrum at the T_{base}. The two inset plots in Fig. 6. (a) and Fig. 6. (b) show the wavelength-drift corrected spectra in the mid-UV and near_IR regions. These pre-flight observations have aided in the correction of the observed on-board wavelength-drift of the LE-LIBS instrument due to various operating temperatures experienced during its one lunar-day operation.

S. Maurice *et al.* [18, 19], R.C. Weins *et al*. [25] and X. Liu *et al.* [27] reported the *influence of working distance* on surface ablation and plasma emission signal response anticipated from a stand-off LIBS instrument with variable (a few meters) working distance. The LE-LIBS instrument, being a fixed close-ranged instrument (as specified in Table I), in principle shall not influence the elemental surface ablation kinetic and instrument response for the design working distance variation of ± 8 mm from 200 mm. However, experiments were carried out to investigate the effect of working distance variation in intervals of ± 2 mm from the design height of 200 mm from the ablation optics unit (AOU). As shown in the Fig. 7. an in-house fabricated sample holder (made of aluminum alloy) comprising a series of circular pockets of diameter 15 mm and depth of 5 mm at varying heights is utilized in these investigations. These pockets are filled with the lunar-regolith simulant powder (*JSC-1A, Orbitec*), and experiments were carried out in a customized 0.4-meter-diameter high vacuum (HV) chamber at a pressure level of ~ 2 x 10^{-4} Pa.

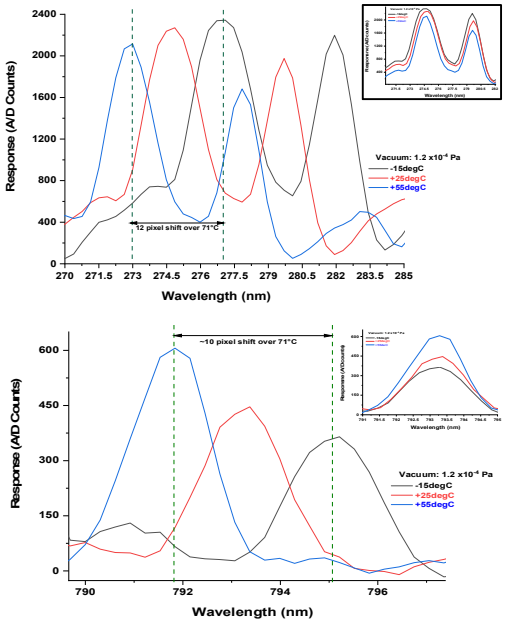

Fig. 6. (a) Mid-UV LIBS spectrum (top) and Fig. 6. (b) near-IR LIBS spectrum (bottom) of the pressed powder disc of the CRM sample SX67-05 as a function of operating temperature at -15 °C (black line), +25 °C (red line), and +55 °C (blue line); Inset of both plots show the wavelength-drift corrected LIBS spectrum

The plasma plume emitting from the soil powder surface (encircled by the white-line trace at the top-right corner of the Fig. 7.) assured the generation of the luminous plasma plume in a high-vacuum environment with a low laser pulse energy of 3.5 mJ. The LIBS emission spectra of the sample at three different sites in each pocket are acquired and five LIBS spectra at each site are recorded. The average of the 15 LIBS spectrums of the sample is analyzed. The performed analysis on the recorded measurements showed very low influence on the spectral response within the Rayleigh length limit of the laser beam (± 4 mm) from 200 mm. At, distances beyond ±4 mm from the design distance, lower number of emission peaks were recorded. This may be due to the decrease in the power density owing to the spreading of the focused laser beam and the effect of the non-zero angle offset between ablation and collection optic units.

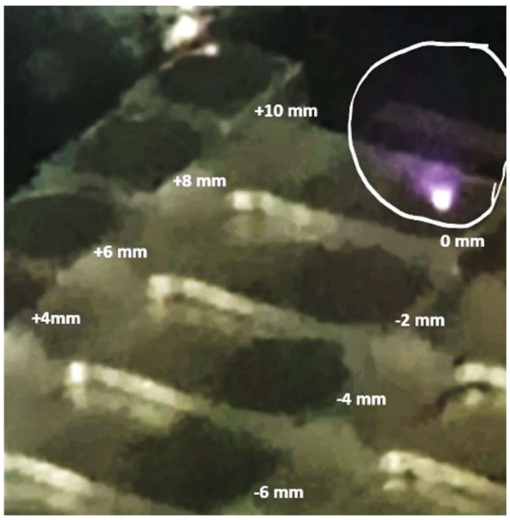

Fig. 7. Sample holder with the JSC-1A powder *(plasma plume in white circle)*

XXXX-XXXX © XXXX IEEE. Personal use is permitted, but republication/redistribution requires IEEE permission.
See http://www.ieee.org/publications_standards/publications/rights/index.html for more information.

Authorized licensed use limited to: KIIT University. Downloaded on December 05,2024 at 14:49:34 UTC from IEEE Xplore. Restrictions apply.
© 2024 IEEE. Personal use is permitted, but republication/redistribution requires IEEE permission. See https://www.ieee.org/publications/rights/index.html for more information.

This article has been accepted for publication in IEEE Sensors Journal. This is the author's version which has not been fully edited and content may change prior to final publication. Citation information: DOI 10.1109/JSEN.2024.3506037

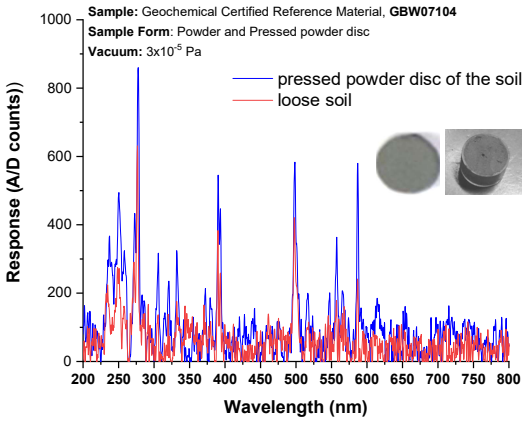

Fig. 8. Overlapped LIBS response plot: Pressed powder disc of soil (blue line), loose soil (red line); Inset shows the snapshots of the sample in its pressed powder disc and loose soil forms.

The spectral response is evaluated further for the *physical form of the target sample*, viz., pellet and loose soil (grain) form. The powdered form of a geochemically certified reference material sample (*GBW07104, Fine Chemical Products*) was made into a circular disc of diameter 13 mm and a thickness of 6 mm. The overlap plot of the spectral (unprocessed spectra) response of the sample in its granular and pressed powder disc form for a single laser shot at +25 °C is shown in Fig. 8. The experiments were performed in high vacuum at a pressure level of $3x10^{-5}$ Pa. The inset of the Fig. 8. portrays the loose soil poured into a tiny cylindrical glass capsule, and the adjacent circular greyish tablet is the pressed disc of the powder. Spectral signatures observed are similar for both forms of the sample; however, the pressed powder disc of the sample in comparison to its powder form produced approximately 1.5 to 2 times more intense LIBS emission spectrum. Our observation was found to be in line with the work reported elsewhere [13, 13, 40]. Although powder form of the sample has yielded a lower intensity spectrum in a high vacuum environment, the single laser-shot-induced surface ablation and measured plasma emission have ensured the possible detection of interesting elements, like, C-I and Na-I at peak wavelengths of 247.87 nm and 568 nm, respectively, along with other major elements detection. This kind of investigation capability may aid in the detection of crucial volatiles on the lunar surface.

D. Data preprocessing Methodology

LIBS spectra are preprocessed to mitigate contributions originating from the intrinsic laser-matter interaction process, experimental parameters, instrument package, and working environment [23-27] prior to performing the analysis. In our work, we have preprocessed the recorded LIBS spectrum to generate a 'clean spectrum (cs)' by removing contributions originating from the ambient background, white noise, and bremsstrahlung continuum and applying correction/correlation factors related to wavelength calibration, operating temperature, wavelength-dependent instrument response, and spectral normalization. Our ground spectral acquisition sequence records the non-laser background (dark or passive) spectrum prior to and immediately after the active spectrum for the same acquisition parameter setting values. This dark spectrum will help to get rid of the influence of ambient illumination and the absorption line characteristics of the solar spectrum. The median of the dark spectra is subtracted from each of the laser-shot-induced plasma emission spectra. This step also eliminates the instrument's offset ADC counts in the range of 450-500 (in digital number, DN). The dark response subtracted LIBS spectrum is processed further for the removal of the overlying noise and the bremsstrahlung continuum. We used the Savizky-Golay (SG) algorithm, a digital smoothening polynomial filter, to remove the white noise in the spectrum. The SG method is used, as this approach aids in to increase the precision of the data without distorting the signal tendency. The asymmetric least squares (ALS) approach is used to perform a baseline creation for the continuum. The ALS algorithm is used in our work, as this methodology needs no prior information about peak shapes or baseline polynomial, and the baseline can be tuned easily with a few parameters without pre-selecting any anchor points that are generally followed in derivative-method based baseline creation. The created baseline is subtracted from the background-corrected and denoised LIBS spectrum. The continuum removal also aids in partial corrections for distance variations, as the baseline in laser-induced plasma emission spectra related to bremsstrahlung and ion-electron recombination is working distance dependent. Our selection and optimization of SG and ALS approaches in comparison to other reported approaches to treat the LIBS spectra acquired in low pressure conditions was communicated elsewhere [36]. Thus the background subtracted, denoised, and baseline removed LIBS emission spectrum is corrected for wavelength drift and instrument response to generate the 'clean spectrum (cs)'. The clean LIBS spectrum was further subjected to the global curve-fitting, peak identification, and peak-centroid estimation procedures [37]. In the case of overlapped emission peaks, in order to disentangle the contribution of other nearby emission lines, a multiple-peak fit (based on Lorentzian function) procedure is applied to find true peak centres. Elemental identification is done by comparing the estimated true peak centres (peak centroids) of the clean LIBS emission spectrum to the emission lines reported in the standard atomic spectral database resources [41, 42]. In addition to these standard atomic spectral databases, as described in the subsequent section, we generated a user database by conducting experiments with flight instrument using discs of pure elements. These investigations gave information about the probable elemental emission lines as recorded by the instrument in a high vacuum environment.

E. Instrument-specific data library generation and Limit of Detection (LoD)

Plasma plume dynamics in low-pressure conditions is different from that of the ambient air environment. Owing to these facts, LIBS-based elemental identification shall be judicious while referring the peak wavelengths and intensities of emission lines with respect to the standard atomic spectral databases. A. Cousin *et al.* [43] work even illustrated the possible wavelength shift of emission lines from air to Mars pressure and reported the generation of instrument-specific spectral library in the required test-environment. In our work, we generated a spectral library in high vacuum at pressure levels of ~$1.5x10^{-4}$ Pa with the flight-LE-LIBS instrument

XXXX-XXXX © XXXX IEEE. Personal use is permitted, but republication/redistribution requires IEEE permission.
See http://www.ieee.org/publications_standards/publications/rights/index.html for more information.

Authorized licensed use limited to: KIIT University. Downloaded on December 05,2024 at 14:49:34 UTC from IEEE Xplore. Restrictions apply.
© 2024 IEEE. Personal use is permitted, but republication/redistribution requires IEEE permission. See https://www.ieee.org/publications/rights/index.html for more information.

This article has been accepted for publication in IEEE Sensors Journal. This is the author's version which has not been fully edited and content may change prior to final publication. Citation information: DOI 10.1109/JSEN.2024.3506037

adapting a similar kind of acquisition approach as close as conceivable to the anticipated ones on-board. ½-inch diameter circular discs of pure metals and their oxides, namely, magnesium, aluminum, silicon, iron, titanium, manganese, chromium, etc., with purity ranging from 99.9% to 99.999% *(GW Metal Technology Co. Ltd.*) were used in the investigation of the probable elemental emission lines. The test setup that was similar to the one shown in Fig. 5. kept inside a 0.4-meter-diameter UHV chamber. The sample surface is perpendicular to the collection axis. The LIBS spectra of the sample were recorded using a laser firing sequence of four single laser shots, two bursts of five laser shots, and one burst of 10 laser shots at a 5 Hz repetition rate, from two to three locations of the same sample. The plasma emission spectrum for every laser fire captured has an acquisition time of one millisecond. As described in Section-III_D, these spectral recordings were subjected to data-preprocessing to produce a clean spectrum free from the overlying noise and intrinsic continuum. Among the 1125 strong lines of the above-mentioned elements (including the element oxygen) in their neutral and first ionization states as per the NIST database [41], 215 lines are observed in the instrument-generated LIBS spectra of the above-listed pure elements. For example, a few significant peaks recorded in the case of elements, viz., Fe, Al, and O, are: 274.51 nm, 319.41 nm, 368.45 nm, and 526.64 nm (Fe), 309.12 nm, 358.72 nm, 624.32 nm, 669.39 nm (Al), 407.37 nm, 436.76 nm, 777.1 nm, and 777.5 nm (O). Measured elemental peak wavelengths were found to vary within ±0.2 nm with respect to the NIST spectral database. This instrument-specific spectral database is further employed in our rapid element search algorithm for the quick elemental search and detection.

The spectral database generation in a high-vacuum environment is further extended with geochemical SRM and CRM samples. These sample standards (*Brammer Standard Company, Inc., Laboratory Chemikal Company, and Fine Chemical Products*) are certified for their physical properties, elemental concentration, and, in most cases, elemental oxide composition. In our experiments, all samples that were originally in powdered form were pressed into circular discs. At the scale of the LE-LIBS spot size (~100-µm diameter FWHM), these pellets are comparatively homogeneous since many granules (> 5 on average) would usually be within this analytical spot. LIBS spectra were acquired from three different sites on each CRM sample pellet's surface. From each sample, thirty LIBS spectra are recorded, and the averaged spectra is subjected to the preprocessing. A non-laser background spectrum was collected prior to each laser shot for the same acquisition time of plasma emission capture. These observations helped us to decode two capability aspects of the instrument; one is to find out the elemental presence for which the signal is low but can still be detected. These observations lead to the assessment of the limit of detection (LOD) of elements. The second capability is towards the estimation of elemental abundances based on the calibration-curve approach. In our work, the minimum elemental composition value at which the emission line is detected without any ambiguity (signal intensity being above the white noise) is considered as the 'LoD'.

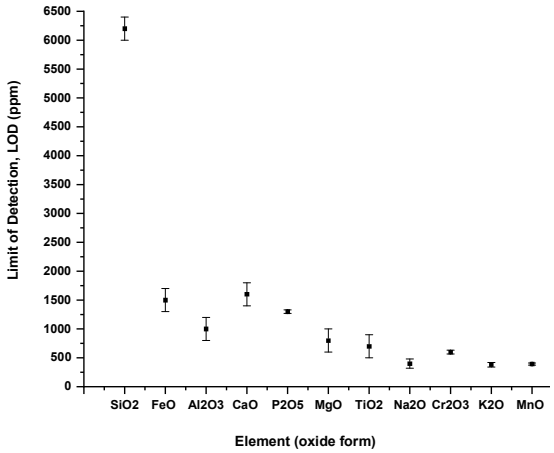

Fig. 9 LoD versus Element oxide

Fig. 9. presents the LoD (in parts-per million) for elements viz., Si, Fe, Al, Ca, Mg, Ti, Na, Cr, K, and Mn. Elemental composition is certified for its oxide form. Elements present in composition (ppm) lower than these reported values cannot be detected by the LE-LIBS instrument. Error bars of the plot correspond to the compositional uncertainty as reported in the certifications of the SRM/CRM sample.

F. Calibration Curves for Elemental Quantification

One of the conventional approaches to determining the abundance of an unknown element is the calibration curve (CC) methodology, which employs the generation of a spectral database in controlled experimental and environmental conditions using geochemical samples of known elemental composition values. The calibration curve corresponds to a particular emission line of the element that is present in spectra of samples, wherein that particular element has a variable composition. This paper outlines the strategy adapted for the spectral database creation, element-specific calibration curve generation, and initial univariate analytical prospects. In this approach, either the peak intensity or the peak area of the emission line relates with the elemental abundance. Owing to its simplicity and ease of interpretation, the univariate approach even had applied to the first LIBS data taken by the Chemcam on Mars from the on-board calibration targets [44]. Our quantitative database generation aimed for the eleven potential elements of interest, i.e., O, Na, Mg, Al, Si, K, Ca, Fe, Ti, Mn, and Cr that are commonly found in lunar rock-forming minerals. The pressed powder pellets of forty geochemical CRMs were used in the generation of calibration curves for the above-listed elements in the high vacuum (~$2x10^{-5}$ Pa). The accuracy of the model is verified by performing leave-one-out analysis on the pre-delivery spectral database. In this paper, we report one such case study performed in the generation of a calibration curve for the element silicon (Si). Table II presents certified major elemental abundances of the chosen SRM and CRM samples for this case study (the suffix 'a' in the table represents the weight of the sample in µg/g). In the Table II, the suffix 'a' represent the weight of the sample in µg/g.

XXXX-XXXX © XXXX IEEE. Personal use is permitted, but republication/redistribution requires IEEE permission.
See http://www.ieee.org/publications_standards/publications/rights/index.html for more information.

Authorized licensed use limited to: KIIT University. Downloaded on December 05,2024 at 14:49:34 UTC from IEEE Xplore. Restrictions apply.
© 2024 IEEE. Personal use is permitted, but republication/redistribution requires IEEE permission. See https://www.ieee.org/publications/rights/index.html for more information.

This article has been accepted for publication in IEEE Sensors Journal. This is the author's version which has not been fully edited and content may change prior to final publication. Citation information: DOI 10.1109/JSEN.2024.3506037

TABLE II
MAJOR ELEMENTAL COMPOSITION STATISTICS OF SRM AND CRM SAMPLES

Elemental Oxide	Sample Nomenclature and Concentration (wt. %)				
	GBW07410	GBW07104	GBW07406	GBW07112	CRM R28
SiO_2	65.64±0.38	60.62±0.14	56.93±0.18	35.69±0.07	5.11± 0.02
Al_2O_3	14.55±0.18	16.17±0.12	21.23±0.16	14.14±0.14	0.37±0.01
Fe_2O_3	4.60±0.13	4.90±0.06	8.09±0.13	24.75±0.084	1.16 ± 0.02^{FeO}
TiO_2	[Ti:0.46±0.03]	[Ti: 3090±90][a]	[Ti:4390±120][a]	7.69±0.09	-
Cao	1.42±0.10	5.20±0.07	0.22±0.03	9.86±0.10	4.09±0.03
MgO	1.25±0.04	1.72±0.06	0.34±0.05	5.25±0.06	0.194±0.005
Na_2O	1.90±0.09	3.86±0.07	0.19±0.02	2.11±0.02	-
K_2O	2.59±0.07	1.89±0.05	1.70±0.06	0.15±0.01	-
MnO	[Mn:706±33][a]	[Mn:604±18][a]	[Mn:1450±82][a]	0.193±0.005	-

LIBS spectra in a high vacuum environment were acquired for thirty laser pulses on each of three distinct sites per sample pellet. Averaged spectra were preprocessed as per the procedure described in Section-III_D. In our univariate quantification approach, normalized line intensity (peak height is normalized with the area under the curve) was used to generate the calibration curve. As mentioned above, four of the five samples signal responses normalized with the peak area are plotted as a function of the element concentration, considering the unaccounted one as the unknown (GBW07104) sample. Fig. 10 shows the calibration curve for the element 'Si' for its emission line at 288.1 nm. For the emission peak at 288.1 nm of the LIBS spectrum from the 'left-out' sample GBW07104, using the linear fit resulted in intercept and slope values; the predicted abundance of the element 'Si' is 27.54 wt.% (certified value: 28.49±0.06 wt.%). The observed uncertainty in the predicted elemental abundance is < 3.5percentage. The 'x-error bar' corresponds to the uncertainty specified in the certified reports, while the 'y-error bar' corresponds to the peak fit, which resulted in uncertainty in the peak height and peak area estimation. Calibration curves for other elements of interest are generated based on the same approach. Our analysis has shown the suitability of the univariate approach for elemental abundance estimation, even for the major elements. This may be due to the presence of a low-level background continuum in a very low-pressure environment. In addition to this conventional approach, we have performed elemental abundance investigations based on the multivariate calibration-free libs (CF-LIBS) approach. Details of these analytical prospects will be communicated elsewhere.

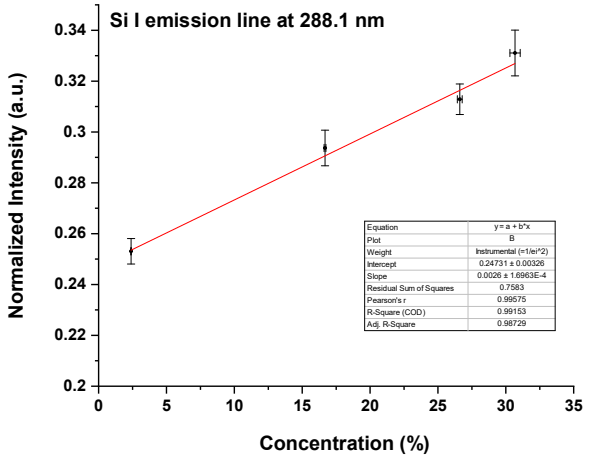

Fig. 10. Calibration curve of 'Si' at 288.1 nm

As reported by the Y. Haung *et al.* [45] on the applicability of machine learning tools for LIBS spectral analysis, our efforts are in progress on the application of machine learning methodologies for LIBS spectral analysis, especially for soil like samples.

IV. Inflight Operations and Observations

Aftermath of the Chandrayaan-3's Vikram lander craft soft landing in the lunar southern high latitude region, in the very early morning hours of August 24, 2023, the Pragyaan rover had its smooth roll-down onto the lunar surface from the lander's ramp platform. The LE-LIBS is operated for the first time on August 25, 2023, at 10:42:21 UTC for a duration of 35 seconds at a southeast site nearly 7 meters away from the Shiv Shakti point. The last powered ON operation was on September 2, 2023, for a duration of 50 seconds on a northeast site that was ~28 meters away from the lander craft. During these 9 days of operations, the instrument's health was normal. This paper details the on-board functionality, operational strategy, acquisition methodologies, and preliminary performance aspects of the instrument.

A. On-board Functionality

The instrument was powered on 66 times, and scientific investigations with diverse acquisition strategies were performed at 25 different sites on the moon surface in the vicinity of the landing point. These sites are the part of a few plain regions, the rim of the craters, the surface disturbed by the rover wheels, etc., along the rover's traverse. The minimum base temperature experienced was +4.5 °C, while the maximum temperature was +25.6 °C, which were well within the design temperature range of the instrument (see Table I). These records are utilized to correct the temperature-dependent wavelength drift of the spectrometer, as per the procedure explained in Section-III_C. The LE-LIBS instrument collected the laser-induced plasma emission signal for more than 750 laser shots. The laser source was operated at pump currents of 95 A and 100 A. The inflight estimated laser pulse energy averaged for 25 shots (based on the output amplitude of the internal feedback photodiode of the laser source, which is sensitive to the laser radiation) at +25 °C base temperature was 3.5 mJ, while the pre-flight measured average laser pulse energy was 3.48 mJ. Fig. 11. presents the radar graph of the average laser energy estimated for different on-board base temperatures of the instrument.

XXXX-XXXX © XXXX IEEE. Personal use is permitted, but republication/redistribution requires IEEE permission.
See http://www.ieee.org/publications_standards/publications/rights/index.html for more information.

Authorized licensed use limited to: KIIT University. Downloaded on December 05,2024 at 14:49:34 UTC from IEEE Xplore. Restrictions apply.
© 2024 IEEE. Personal use is permitted, but republication/redistribution requires IEEE permission. See https://www.ieee.org/publications/rights/index.html for more information.

This article has been accepted for publication in IEEE Sensors Journal. This is the author's version which has not been fully edited and content may change prior to final publication. Citation information: DOI 10.1109/JSEN.2024.3506037

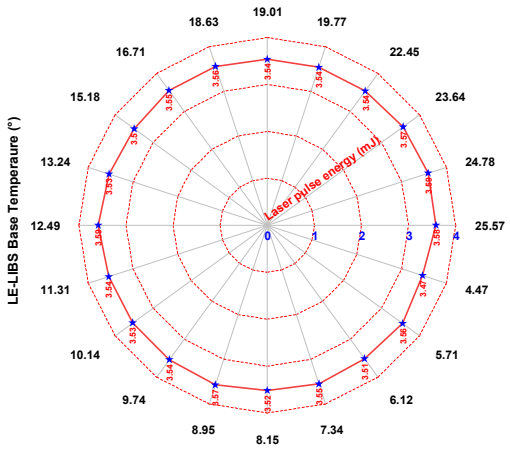

Fig. 11. Laser pulse energy (avg.) vs. LE-LIBS base temperature

B. Operational Strategy and Spectral Acquisition

At first, scientifically interesting sites are selected from the images recorded by the NavCam (navigation camera) of the rover. Once the rover reaches near that site and stops, the LIBS instrument shoots down 4-laser pulses at a 5 Hz repetition rate. The laser-induced plasma emission signal was recorded for every laser shot. A non-laser background (dark/passive) signal was acquired at the same site for the same integration time prior to the plasma emission acquisition. Fig. 12. presents the adapted on-board operational strategy. As seen in the chart, in the normal operational strategy, during the power ON, the LIBS instrument operates two times by sending four laser pulses each time. 'LIBS_POST Operation; will be initiated based on the spectral quality obtained in the 'LIB_PRE Operation chain'. During the initial phases of on-board operations, 'LIBS_POST Operation' was repetitive of the 'LIBS_PRE Operation' at the same site for the same commanded measurement parameter values. However, in later experiments, 'LIBS_POST Operation' was executed with different delay times, integration times, and spectral acquisition methodologies. Two kinds of spectral acquisition methodology are adopted, i.e., i) paired spectral registration (PSR) and ii) grouped spectral registration (GSR). In the first case, background signal was captured before each laser shot fired, and the same sequence (01, 01, 01…, '0'-no-laser fire, '1'-laser fire) is followed for subsequent laser fires. In the GSR case, a bunch of laser shots (3, 5, 10, 15, 20 etc.) were fired and non-laser background was acquired before the first and last laser shots (01110, 0111110..., '0'-no-laser fire, '1'-laser fire). A total of 500 plus non-laser background spectra were acquired during the operational lifetime of the instrument. Moreover, the LE-LIBS was operated in two modes, viz., OLM (Open Loop Mode) and CLM (Close Loop Mode). In the OLM, the spectral acquisition window started before the laser fire, while in the CLM, the spectral acquisition within the set integration time window was realized after a certain delay time with respect to the laser pulse output time. The latter mode of operation might aid in assessing the influence of the background continuum (resulting because of ion-electron recombination and bremsstrahlung processes) on the plasma signal, if any.

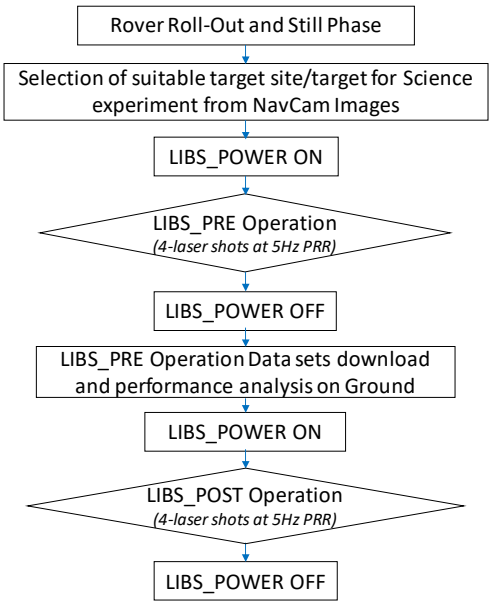
Rover Roll-Out and Still Phase
Selection of suitable target site/target for Science experiment from NavCam Images
LIBS_POWER ON
LIBS_PRE Operation
(4-laser shots at 5Hz PRR)
LIBS_POWER OFF
LIBS_PRE Operation Data sets download and performance analysis on Ground
LIBS_POWER ON
LIBS_POST Operation
(4-laser shots at 5Hz PRR)
LIBS_POWER OFF

Fig 12: On-board operational strategy of the LIBS sensor

Most of the operations carried out by the LE-LIBS instrument were in the OLM category. The LIBS instrument raw data, calibration files, correction factors, etc., can be accessed from the Chandrayaan-3 portal of the ISRO Science Data Archive (https://pradan.issdc.gov.in/ch3).

C. Preliminary Results and Discussion

The illumination conditions, target site nature, and the rover body plane tilts had resulted in various kinds of non-laser background and laser-induced plasma emission spectral signatures. A few of the operations were found resulting in a flat background, while for a few, the non-laser background was saturated. Similarly, acquired plasma emission spectra too had shown different signatures, a few spectra populated with intense emission peaks and a few having a very low number of emission peaks (dominated by the non-laser background). Fig. 13. shows the partially processed spectral-stack plot of the laser-induced plasma emission response (blue line) of the lunar regolith and the non-laser background response (red line) for 3-successive measurements performed on the 27th day of August 2023 at the time of 18.12.23 UT. The LE-LIBS sensor functioned in open loop mode of operation at 5 Hz pulse repetition rate of the laser source for the integration time of one millisecond. Fig. 14. presents the integrated plasma emission spectrum (of the spectral stack shown in the Fig. 13.) with the labels on the emission peaks describing the first-cut elemental findings. Prior to the elemental search, this spectrum was subjected to the partial data treatment processes, viz., temperature dependent wavelength drift, non-laser background subtraction, and denoising, and is subsequently transferred to the peak finding, global curve fitting, peak centroid computation, element search, and assignment logics to obtain the elemental findings. The centroids of the emission peaks of the spectrum are cross-matched (within 1-pixel resolution, ±0.35 nm) with the reference strong, persistent, and most probable wavelengths from the standard atomic spectral database resources to identify elements.

XXXX-XXXX © XXXX IEEE. Personal use is permitted, but republication/redistribution requires IEEE permission.
See http://www.ieee.org/publications_standards/publications/rights/index.html for more information.

Authorized licensed use limited to: KIIT University. Downloaded on December 05,2024 at 14:49:34 UTC from IEEE Xplore. Restrictions apply.
© 2024 IEEE. Personal use is permitted, but republication/redistribution requires IEEE permission. See https://www.ieee.org/publications/rights/index.html for more information.

This article has been accepted for publication in IEEE Sensors Journal. This is the author's version which has not been fully edited and content may change prior to final publication. Citation information: DOI 10.1109/JSEN.2024.3506037

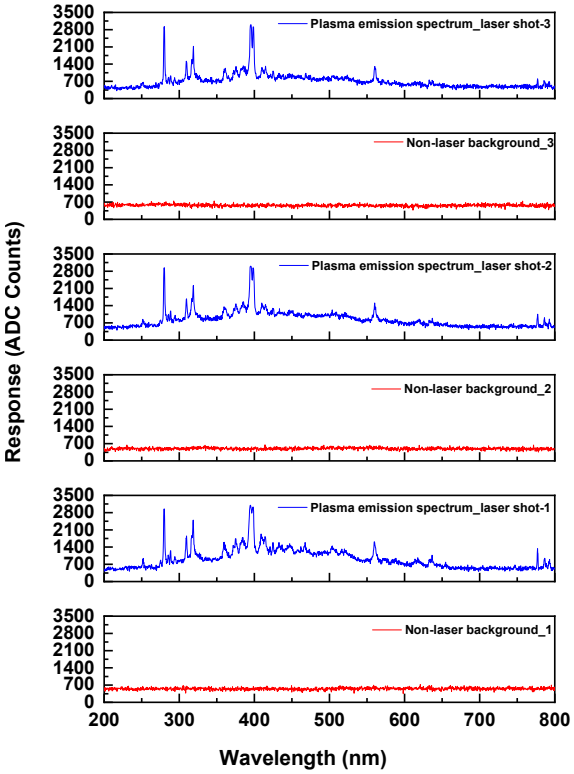

Fig. 13. Non-laser background (red line) and laser pulse-induced plasma emission spectra (blue line) of the lunar-regolith for three successive measurements, Date of operation on the Moon: 27 August 2023

Our preliminary analysis of the LIBS emission spectrum (integrated for 3-laser shots) of the lunar regolith under afore-mentioned operational conditions has indicated the presence of elements, namely, oxygen (O), magnesium (Mg), aluminum (Al), silicon (Si), calcium (Ca), iron (Fe), titanium (Ti), chromium (Cr), and manganese (Mn). The performed first-cut elemental analysis on the mentioned data records of the LIBS payload operation on the Moon has revealed the dominance of elements viz., Ca, Al, and Fe along with Si and O, followed by elements like Mg, Ti, Mn, and Cr. These findings may hint at the presence of Ca, Mg-rich aluminum silicate minerals (like anorthosite minerals) and low-Ti magnesium silicate minerals in the high southern-latitude region of the Moon. Detailed analyses of all the LE-LIBS data records aboard the Pragyaan rover are underway to investigate further significant findings, including the possible detection of volatile elements like helium (He), carbon (C), nitrogen (N), phosphorous (P), and sulphur (S), etc. Such findings may play a crucial role in investigating the source, transport, and loss mechanisms of other volatiles, as well as the relationship between lunar soil and the ancient solar wind. Further, it may aid the lunar geologist to evaluate whether the moon was derived from the proto-earth and whether the volatile depletion can be attributed to volatility or core formation. Table III presents a list of line wavelengths observed in the laser-induced plasma spectrum of the lunar regolith, along with details of identified elemental species and their respective transition energy levels.

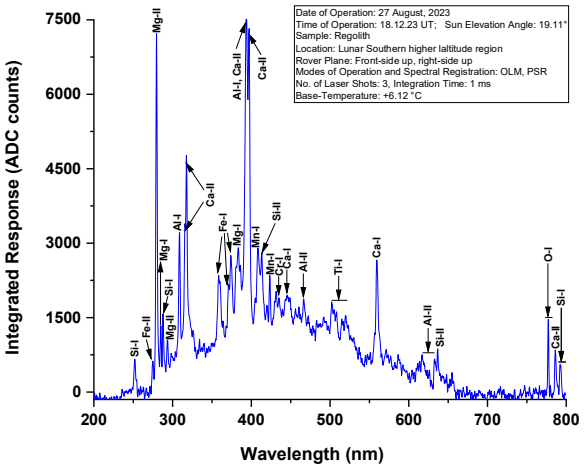
Date of Operation: 27 August, 2023
Time of Operation: 18.12.23 UT; Sun Elevation Angle: 19.11°
Sample: Regolith
Location: Lunar Southern higher lattitude region
Rover Plane: Front-side up, right-side up
Modes of Operation and Spectral Registration: OLM, PSR
No. of Laser Shots: 3, Integration Time: 1 ms
Base-Temperature: +6.12 °C
Integrated Response (ADC counts)
Wavelength (nm)

Fig. 14. Background-subtracted, denoised, and integrated (for 3-shots) LIBS spectrum of the lunar regolith with elemental findings *(partially processed spectrum)*.

TABLE III
LIST OF SIGINFICANT EMISSION LINES AND IDENTIFIED ELEMETNS FROM LIBS SPECTRUM OF THE LUNAR REGOLITH

Species	Measured Peak Wavelengths (nm)	Matched Reference Wavelengths (nm)	Transition Energy Levels term
O I	777.16	777.19	$^5S^\circ_2$-$^5P_3$
	777.54	777.53	$^5S^\circ_2$-$^5P_1$
Mg I	285.46	285.21	$^1S_0$-$^1P^\circ_1$
	383.43	383.23	$^3P^\circ_2$-$^3D_2$
Mg II	279.56	279.55	$^2S_{1/2}$-$^2P^\circ_{3/2}$
	293.47	293.65	$^2P^\circ_{3/2}$-$^2S_{1/2}$
Al I	308.65	308.21	$^2P^\circ_{1/2}$-$^2D_{3/2}$
	394.50	394.40	$^2P^\circ_{1/2}$-$^2S_{1/2}$
Al II	466.46	466.3	$^1D_2$-$^1P^\circ_1$
	618.27	618.16	$^3F^\circ_2$-$^3G_3$
	633.62	633.57	$^1D_2$-$^1P^\circ_1$
Si I	251.99	251.92	$^3P_2$-$^3P^\circ_1$
	288.22	288.16	$^1D_2$-$^1P^\circ_1$
	791.90	791.84	$^3D_1$-$^3F^\circ_2$
	793.15	793.23	$^3D_2$-$^3F^\circ_3$
Si II	413.11	413.09	$^2D_{5/2}$-$^2F^\circ_{7/2}$
	636.84	637.13	$^2S_{1/2}$-$^2P^\circ_{1/2}$
Ca I	445.50	445.48	$^3P^\circ_2$-$^3D_3$
	560.36	560.28	$^3D_2$-$^3D^\circ_1$
Ca II	315.76	315.89	$^2P^\circ_{1/2}$-$^2D_{3/2}$
	317.65	317.93	$^2P^\circ_{3/2}$-$^2D_{3/2}$
	393.16	393.36	$^2S_{1/2}$-$^2P^\circ_{3/2}$
	396.91	396.84	$^2S_{1/2}$-$^2P^\circ_{1/2}$
	785.98	785.97	$^2P^\circ_{3/2}$-$^2D_{5/2}$
Fe I	358.77	358.69	a^5F_2-$z^5G^\circ_2$
	371.44	371.99	a^5D_4-$z^5F^\circ_5$
	374.20	374.55	a^5D_2-$z^5F^\circ_3$
Fe II	274.77	274.93	$a^4D_{5/2}$-$z^4F^\circ_{7/2}$
Ti I	503.73	503.64	b^3F_3- $w^3G^\circ_4$
	506.37	506.46	a^3F_4- $z^3D^\circ_3$
	520.98	521.04	a^3F_4- $z^3F^\circ_4$
Cr I	435.14	435.17	a^5D_4-$z^5F^\circ_5$
Mn I	408.32	408.36	$a^6D_{5/2}$-$z^6D^\circ_{7/2}$
	423.55	423.53	$a^4D_{7/2}$-$y^4P^\circ_{5/2}$
	449.07	450.22	$a^4D_{1/2}$-$z^4D^\circ_{3/2}$

V. Conclusion

The miniaturized low-energy eye-safe laser excitation-based LIBS instrument (LE-LIBS) aboard the Chandrayaan-3 Pragyaan rover is the first-of-its-kind to operate and perform in-situ investigations on the Moon from a close distance of

XXXX-XXXX © XXXX IEEE. Personal use is permitted, but republication/redistribution requires IEEE permission.
See http://www.ieee.org/publications_standards/publications/rights/index.html for more information.

Authorized licensed use limited to: KIIT University. Downloaded on December 05,2024 at 14:49:34 UTC from IEEE Xplore. Restrictions apply.
© 2024 IEEE. Personal use is permitted, but republication/redistribution requires IEEE permission. See https://www.ieee.org/publications/rights/index.html for more information.

This article has been accepted for publication in IEEE Sensors Journal. This is the author's version which has not been fully edited and content may change prior to final publication. Citation information: DOI 10.1109/JSEN.2024.3506037

200 mm. The work reported describes crucial preflight investigations carried out for the validation of the instrument's functionality and performance in a high vacuum environment at a pressure level in the range of 10^{-4}-10^{-5} Pa. The performed spectrometric calibration resulted in a minimal variation of about $\leq 1/10^{th}$ of a pixel at an average between the predicted wavelengths and calibrated source emission wavelengths.

Influence of operating temperature, working distance, and sample form (pressed powder soil, loose soil) on the instrument's functionality and performance were studied. The estimated wavelength drift per °C temperature is ≤ 0.15 pixel. The instrument response does not appear to vary much within the design working distance tolerance of ±8 mm. Our investigations have also shown the LIBS signal strength enhancement of 1.5 to 2 times for the pressed powder disc form of the sample in comparison to its powder form. A single laser-shot LIBS spectrum was found suitable for detection of major and minor elements. The luminous plasma plume core emanating from the lunar regolith simulant powder (JSC-1A) surface ascertained the potentiality of the low-energy LIBS technique under low-pressure conditions. Aspects related to the need for the instrument-specific data library and the methodology are presented. We have described an overview of the realized spectral acquisition sequence and data preprocessing methodology and shown the suitability of the univariate calibration method in retrieving the elemental abundance from the generated calibration curve for the element silicon at the peak wavelength of 288.1 nm. The resulted percentage of uncertainty in estimated abundance for 'Si' is < 3.5 percentage. The extensively performed pre-flight calibration and characterization studies and the database generated with the instrument prior to its voyage had substantially aided the analysis of the LIBS data collected on board the Chandrayaan-3 Pragyaan rover. On August 25, 2023, the first operation of the LE-LIBS instrument was carried out on a site a couple of meters away from the Vikram lander. During its nine-day operation, the investigations performed on nearly 25 different sites at various locations along the total rover-traversed path of about 103 meters, resulted in a good amount of data to infer the elemental composition in the lunar southern high latitude region surrounding the 'Shiv Shakti' point. The LE-LIBS has collected a total of 500+ non-laser background spectra and sent more than 750 laser shots to record the laser-induced plasma emission signal from the lunar regolith. Our preliminary analysis of the reported LIBS emission spectrum of the lunar regolith has indicated the presence of elements, viz., O, Mg, Al, Si, Ca, Fe, Ti, Cr, and Mn, hinting at the possible presence of Ca, Mg-rich aluminum silicate minerals, and low-Ti magnesium silicate minerals in high lunar southern-latitude regions. Subsequent spectral analysis found even more promising in terms of a few vital trace and volatile elements identifications, which will be communicated shortly. These findings may be useful for the betterment of understanding the source, transport, and loss mechanism of volatiles in near-polar regions. Overall, the development and successful operations of the LE-LIBS instrument have proven its capability to function in a harsh ultra-high vacuum environment as an effective in-situ close-range analytical tool on planetary surfaces.

VI. Acknowledgements

The authors are thankful to the management of the Laboratory for Electro-Optics Systems, ISRO, for their encouragement in the development phases of the LIBS instrument for low-pressure environment applications. We are grateful to Mr. A.S. Kiran Kumar (former Chairman, ISRO), Dr. S. Somanath (Chairman, ISRO), and Mr. M. Sankaran (Director, U R Rao Satellite Centre) for their support and valuable insights during on-board operational phases of the instrument. We extend our gratitude to Mr. Pramod K.B., Mr. Umesh S.B., and Mr. S.P. Karanth, the executives of the Environment Test Facility and Photonics Systems Area at LEOS, for their suggestions related to crucial performance tests. The authors also acknowledge the support from the other members of the instrument development team at LEOS, the Chandrayaan-3 team from different ISRO centres, URSC, ISTRAC, and SAC, for the successful commissioning and execution of LE-LIBS instrument operations on the Moon.

VII. Data Availability

LIBS on-board raw and calibrated data records, along with necessary ground-generated correction/correlation factors, calibration files, are available publicly at the ISSDC (ISRO Space Science Data Center) portal of the ISRO at https://pradan.issdc.gov.in/ch3 from 23 August 2024.

VIII. References

[1] Clayton S.C. Yang et al., "Raman and UVN+LWIR LIBS detection system for in-situ surface chemical identification", *MethodsX,* vol. 9, 101647, 2022, https://doi.org/10.1016/j.mex.2022.101647.

[2] N. Tarcea et al, "Raman spectroscopy-a powerful tool for in situ planetary science", *Space Science Reviews*, vol. 135, p. 281-292, 2008, https://doi.org/10.1007/s11214-007.9729-y

[3] R. Rieder et al., "The chemical composition of Martian soil and rocks returned by the mobile alpha proton X-ray spectrometer: preliminary results from the X-ray mode", *Science*, vol. 278, no. 5344, p. 1771-1774, 1997, https://doi.org/10.1126/science.278.5344.1771

[4] S.V. Vadawale, N.P.S. Mithun, M. Shanmugam, et al. "Chandrayaan-3 APXS elemental abundance measurements at lunar high latitude", *Nature*, 2024, https://doi.org/10.1038/s41586-024-07870-7.

[5] D.A. Cremers, F.Y. Yueh, J. P. Singh, and H. Zhang. "Laser-Induced Breakdown Spectroscopy," Elemental Analysis. *Wiley Online Library*, 2006, doi:10.1002/0470093013

[6] A.K.Myakalwar, et al., "LIBS as a Spectral Sensor for Monitoring Metallic Molten Phase in Metallurgical Applications - A Review", *Minerals,* vol. 11, no. 1073, 2021, https://doi.org/10.3390/min11101073.

[7] David W. Hahn, and Nicoló Omenetto, "Laser-induced breakdown spectroscopy (LIBS), part II: review of instrumental and methodological approaches to material analysis and applications to different fields", *Applied spectroscop*y, Vol. 66, no. 4, p. 347-419, 2012, https://doi.org/10.1366/11-06574

[8] F. C. DeLucia *et al*., "Laser-induced breakdown spectroscopy (LIBS): a promising versatile chemical sensor technology for hazardous material detection," *IEEE Sensors Journal*, vol. 5, no. 4, pp. 681-689, 2005, https://do.org/10.1109/JSEN.2005.848151.

[9] A.K. Knight, N.L. Scherbarth, D.A. Cremers and M.J. Ferris, "Characterization of Laser-Induced Breakdown Spectroscopy (LIBS) for Application to Space Exploration", *Applied Spectroscopy*, vol. 54, no. 3, p. 331-340, 2000, doi:10.1366/0003702001949591

[10] J. Thompson, R. Wiens et al., "Remote laser-induced breakdown spectroscopy analyses of Dar al Gani 476 and Zagami Martian meteorites", *Journal of Geophysical Research*. vol. 111, 2006, https://doi.org/10.1029/2005JE002578

[11] F. Colao, R. Fantoni, V. Lazic, A. Paolini, F. Fabbri, G.G. Ori, L. Marinangeli, A. Baliva, "Investigation of LIBS feasibility for in situ

XXXX-XXXX © XXXX IEEE. Personal use is permitted, but republication/redistribution requires IEEE permission.
See http://www.ieee.org/publications_standards/publications/rights/index.html for more information.

Authorized licensed use limited to: KIIT University. Downloaded on December 05,2024 at 14:49:34 UTC from IEEE Xplore. Restrictions apply.
© 2024 IEEE. Personal use is permitted, but republication/redistribution requires IEEE permission. See https://www.ieee.org/publications/rights/index.html for more information.

This article has been accepted for publication in IEEE Sensors Journal. This is the author's version which has not been fully edited and
content may change prior to final publication. Citation information: DOI 10.1109/JSEN.2024.3506037

planetary exploration: An analysis on Martian rock analogues", P*lanetary and Space Science,* vol. 52, no. 1–3, p. 117-123, 2004, https://doi.org/10.1016/j.pss.2003.08.012

[12] P. Lehner *et al*., "Mobile Manipulation of a Laser-induced Breakdown Spectrometer for Planetary Exploration," *2023 IEEE Aerospace Conference*, Big Sky, MT, USA, 2023, pp. 1-19, doi:10.1109/AERO55745.2023.10115597.

[13] J. Lasue, R.C. Wiens, S.M. Clegg, D.T. Vaniman, K.H. Joy, S. Humphries, A. Mezzacappa, N. Melikechi, R.E. McInroy, and S. Bender, "Remote Laser-Induced Breakdown Spectroscopy (LIBS) for Lunar Exploration", J. *Geophys. Res. (Planets)*, vol. 117, no. 1, E01002, p. 1–18, 2012, https://doi.org/10.1029/2011JE003898.

[14] Jobin K. Antony, S.J. Gurneesh, Nilesh J. Vasa, , V.L.N Sridhar Raja, A.S. Laxmiprasad, "Modelling of laser-induced breakdown spectroscopy for very low pressure conditions", A*ppl. Phys.A*, vol. 101, p. 161-165, 2010, https://doi.org/10.1007/s00339-010-5782-1

[15] R. Shu, H. Qi, G. Lu, D. Ma, Z. He, and Y. Xue, "Laser-induced breakdown spectroscopy based detection of lunar soil simulants for moon exploration", *Chin. Opt. Lett*., vol. 5, no. 1, p. 58–59, 2007.

[16] B. Sallé, D.A. Cremers, S. Maurice, and R.C. Wiens, "Laser induced breakdown spectroscopy for space exploration applications: Influence of the ambient pressure on the calibration curves prepared from soil and clay samples", S*pectrochim. Acta B,* vol. 60, p. 479–490, 2005, https://doi.org/10.1016/j.sab.2005.02.009

[17] M. Kuzuya, H. Matsumoto, H. Takechi, O. Mikami, "Effect of Laser Energy and Atmosphere on the Emission Characteristics of Laser-Induced Plasmas", *Applied Spectroscopy*, vol. 47, no. 10, p. 1659-1664, 1993, https://doi.org/10.1366/0003702934334804

[18] S. Maurice, et al., :The ChemCam Instrument Suite on the Mars Science Laboratory (MSL) Rover: Science Objectives and Mast Unit Descriptio"n, S*pace Science Reviews,* vol. 170, 2012, https://doi.org/10.1007/s11214-012-9912-2.

[19] S. Maurice, R.C. Wiens, P. Bernardi *et al.,* "The SuperCam Instrument Suite on the Mars 2020 Rover: Science Objectives and Mast-Unit Description", *Space Sci Rev*, vol. 217, no. 47, 2021, https://doi.org/10.1007/s11214-021-00807-w

[20] W. Xu, et al., "The MarSCoDe Instrument Suite on the Mars Rover of China's Tianwen-1 Mission", *Space Science Reviews*, vol. 217, no. 5, 2021, https://doi.org/10.1007/s11214-021-00836-5

[21] A.S. Laxmiprasad, R.V.L.N. Sridhar, Adwaita Goswami et al., "Laser Induced Breakdown Spectroscope on Chandrayaan-2 Rover: A Miniaturized Mid-UV to Visible Active Spectrometer for Lunar Surface Chemistry Studies", *Current science,* vol. 118, p. 573-581, 2020, https://doi.org/10.18520/cs/v118/i4/573-581.

[22] D.S. Vogt, S. Schröder, L. Richter, M. Deiml, P. Webels, J. Neumann, H.-W.Hübers, "VOILA on the LUVMI-X Rover: Laser-Induced Breakdown Spectroscopy for the Detection of Volatiles at the Lunar South Pole", *Sensors*, vol. 22, no. 9518, 2022, https://doi.org/10.3390/s22239518

[23] J.A. Aguilera, C. Aragón, V. Madurga, J. Manrique, "Study of matrix effects in laser induced breakdown spectroscopy on metallic samples using plasma characterization by emission spectroscopy", S*pectrochimica Acta Part B: Atomic Spectroscopy*, vol. 64, no. 10, p. 993-998, 2009, https://doi.org/10.1016/j.sab.2009.07.007.

[24] A.S. Eppler, D.A. Cremers, D.D. Hickmott, M.J. Ferris, and A.C. Koskelo, "Matrix effects in the detection of pb and ba in soils using laser-induced breakdown spectroscopy", *Applied Spectroscopy*, vol. 50, no. 9, 1996 , https://doi.org/10.1366/0003702963905123

[25] R.C. Wiens et al., "Pre-flight calibration and initial data processing for the ChemCam laser-induced breakdown spectroscopy instrument on the Mars Science Laboratory rover", *Spectrochimica Acta Part B*, vol. 82, p. 1–27, 2013, http://dx.doi.org/10.1016/j.sab.2013.02.003

[26] Carey Legett et al., "Optical calibration of the SuperCam instrument body unit spectrometers", *Applied Optics*, vol. 61, no. 11, 2022, https://doi.org/10.1364/AO.447680

[27] X. Liu, et al., :Development and Testing of the MarSCoDe LIBS Calibration Target in China's Tianwen-1 Mars Mission", *Space Science Reviews*, vol. 219, no. 5, 2023, https://doi.org/10.1007/s11214-023-00987-7.

[28] Chandrayaan-3: Advancements in lunar exploration science, News, *Current Science,* 2023, https://www.currentscience.ac.in/Volumes/125/07/0709.pdf

[29] Yue Cheng. et al., "Spectral properties of ultra-low thermal expansion Er3+/Yb3+ co-doped phosphate glasses", *Ceramics International,* vol. 49, no. 11, p. 18305-18310, 2023, https://doi.org/10.1016/j.ceramint.2023.02.202

[30] Aroua Langar, Chaker Bouzidi, Habib Elhouichet, Mokhtar Férid, "Er–Yb codoped phosphate glasses with improved gain characteristics for an efficient 1.55µm broadband optical amplifiers", *Journal of Luminescence,* vol. 148, p. 249-255, 2014, ISSN 0022-2313, https://doi.org/10.1016/j.jlumin.2013.12.008.

[31] M. Silver et al., "Novel, ultra-compact, high-performance, eye-safe laser rangefinder for demanding applications", *Proc. SPIE, Laser Radar Technology and Applications XXI*, 98320R, 2016, https://doi.org/10.1117/12.2222986.

[32] Marco Vitiello, Andrea Pizzarulli, and Andrea Ruffini, "A compact high power Er:Yb:glass eyesafe laser for infrared remote sensing applications", *Proc. SPIE, Technologies for Optical Countermeasures VII*, 78360C, 2010, https://doi.org/10.1117/12.864673

[33] A. E. Hussein, P. K. Diwakar, S. S. Harilal, A. Hassanein, "The role of laser wavelength on plasma generation and expansion of ablation plumes in air". *J. Appl. Phys.,* vol. 113, no. 14, 143305, 2013, https://doi.org/10.1063/1.4800925.

[34] V.N. Rai and S.N. Thakur, "Physics of plasma in laser-induced breakdown spectroscopy, Chapter-IV", *Elsevier,* 2007, https://doi.org/10.1016/B978-044451734-0.50007-7.

[35] A.S. Laxmiprasad, et al., "An in situ laser induced breakdown spectroscope (LIBS) for Chandrayaan-2 rover: Ablation kinetics and emissivity estimations", *Advances in Space Research,* vol. 52, no. 2, p. 332–341, 2013, https://doi.org/10.1016/j.asr.2013.03.021.

[36] R.V.L N. Sridhar et al., "Denoising and Baseline Correction Prospects of Laser Induced Plasma Spectra acquired under Low Pressure Conditions: Comparison of Algorithms and Optimization Perspectives", *2021 IEEE International Conference on Electronics, Computing and Communication Technologies (CONECCT)*, Bengaluru, India, p. 01-04, 2021, https://doi.org/10.1109/CONECCT52877.2021.9622605.

[37] R.V.L.N. Sridhar et al., "An Automatic Peak Finding and Fitting Aspects of Laser Induced Plasma Spectra acquired in High Vacuum: Tradeoff Simulations and Statistics", *2022 IEEE International Conference on Electronics, Computing and Communication Technologies (CONECCT), Bengaluru,* India, *p*. 1-5, 2022, https://doi.org/10.1109/CONECCT55679.2022.9865112.

[38] Wojciech Gromelski and Pawel Gasior, "Absolute calibration of LIBS data, Proc. SPIE 10808, Photonics Applications in Astronomy, Communications, Industry and High Energy Physics Experiments", 2018 , 108080M, https://doi.org/10.1117/12.2501506.

[39] Prashanth Kumar et al., 'Quantitative estimation of elemental composition employing a synthetic generated spectrum', *Applied Optics*, vol. 57, no. 19, p. 5443-5440, 2018, https://doi.org/10.1364/AO.57.005443.

[40] Stehrer, T. et al. "Laser-induced breakdown spectroscopy of iron oxide powder", *Journal of Analytical Atomic Spectrometry*, vol. 24, no.7, p. 973-978, 2009, https://doi.org/10.1039/B817279

[41] A. Kramida, Yu. Ralchenko, J. Reader, and NIST ASD Team, "NIST Atomic Spectra Database", version 5.11, 2023, DOI: https://doi.org/10.18434/T4W30F

[42] L. Kurucz atomic linelist; editing status 2022-04-06; re3data.org - Registry of Research Data Repositories, 2023, http://doi.org/10.17616/R3977N

[43] D A. Cousin et al., "Laser induced breakdown spectroscopy library for the Martian environment", *Spectrochimica Acta Part B,* vol. 66, p. 805–814, 2011, https://doi.org/10.1016/j.sab.2011.10.004.

[44] C. Fabre et al., "In situ calibration using univariate analyses based on the onboard ChemCam targets: first prediction of Martian rock and soil compositions", *Spectrochimica Acta Part B: Atomic Spectroscopy*, vol. 99, p. 34-51, 2014, ISSN0584-8547, https://doi.org/10.1016/j.sab.2014.03.014.

[45] Yingchao Huang, Sivanandan S. Harilal, Abdul Bais, Amina E. Hussein, "Progress toward Machine Learning Methodologies for Laser-Induced Breakdown Spectroscopy with an Emphasis on Soil Analysis", *IEEE Transactions on Plasma Science*, vol. 51, no. 7, p. 1729-1749, 2023, https://doi.org/10.1109/TPS.2022.3231985.

XXXX-XXXX © XXXX IEEE. Personal use is permitted, but republication/redistribution requires IEEE permission.
See http://www.ieee.org/publications_standards/publications/rights/index.html for more information.

Authorized licensed use limited to: KIIT University. Downloaded on December 05,2024 at 14:49:34 UTC from IEEE Xplore. Restrictions apply.
© 2024 IEEE. Personal use is permitted, but republication/redistribution requires IEEE permission. See https://www.ieee.org/publications/rights/index.html for more information.

This article has been accepted for publication in IEEE Sensors Journal. This is the author's version which has not been fully edited and content may change prior to final publication. Citation information: DOI 10.1109/JSEN.2024.3506037

R.V.L.N. Sridhar was awarded his M.Tech degree in the Laser Technology Programme from the Indian Institute of Technology, Kanpur (IITK) in 2004 and has obtained his M.Sc. degree in Physics from the Acharya Nagarjuna University P.G. Centre, Andhra Pradesh, in 2000. He has been working in the Laser Systems and Instrumentation Group of LEOS, ISRO, since 2006. His main areas of interest are system engineering, instrumentation, and data analytics catering to laser-based instrument development for space applications. He is the principal investigator of the LIBS instrument flown in the Pragyaan rover, Chandrayaan-3 mission.

Adwaita Goswami has obtained his Bachelor Degree in Instrumentation and Electronics Engineering from Jadavpur University, Kolkata. He has been working in the Laser Systems and Instrumentation Group of LEOS, ISRO, since 2004. His main areas of interest are electronics system engineering and development catering to instrument development for interplanetary missions. He is the system engineer for the LIBS instrument flown in the Chandrayaan-3 Pragyaan rover.

K.A. Lohar is an opto-mechanical system engineer with the expertise in the field of design, assembly, and alignment of opto-mechanical systems. He has obtained his M.Tech degree from BMS College of Engineering, Bengaluru. He has been working in the Mechanical Systems Group of the LEOS-ISRO since 1994. He is the principal mechanical system designer for the LIBS instrument aboard the Chandrayaan-3 Pragyaan rover.

S. Malathi completed her Ph.D. from the Indian Institute of Science (IISc.), Bangalore. She is the principal investigator and co-principal investigator for several projects funded by the DST, RESPOND, and AR&DB. After her 10-year successful stint as a faculty member at the M.S. Ramaiah University of Applied Sciences, Bengaluru, she is currently working as a professor in the department of Electronics and Communication Engineering, Graphic Era (Deemed to be) University, Dehradun, India.

K.V. Sriram has obtained his Ph.D. from the Indian Institute of Technology, Madras (IITM). He spearheaded the optics developments at LEOS and led the development of meter-class super-lightweight high-performance telescopes, multi-band optics, super-polished optics, and SiC optics for ISRO space missions. His expertise includes the development of large-aperture high-resolution optical systems, multi-element lens assembly manufacturing and testing, high-precision optical alignment, interferometric testing, and the characterization of space optical systems. He is a "Distinguished Fellow of the Optical Society of India" and currently the Director of LEOS.

XXXX-XXXX © XXXX IEEE. Personal use is permitted, but republication/redistribution requires IEEE permission.
See http://www.ieee.org/publications_standards/publications/rights/index.html for more information.

Authorized licensed use limited to: KIIT University. Downloaded on December 05,2024 at 14:49:34 UTC from IEEE Xplore. Restrictions apply.
© 2024 IEEE. Personal use is permitted, but republication/redistribution requires IEEE permission. See https://www.ieee.org/publications/rights/index.html for more information.